

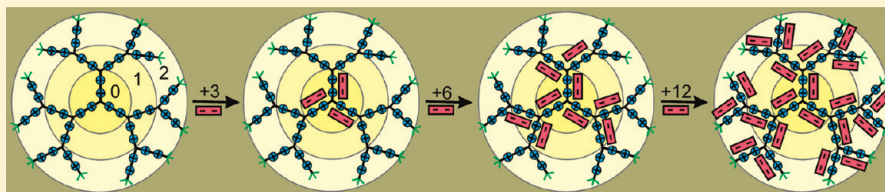
Shell-by-Shell Inside-Out Complexation of Organic Anions in Flexible and Rigid Pyridinium Dendrimers

Murugavel Kathiresan and Lorenz Walder*

Institute of Chemistry OCII, University of Osnabrueck, Barbarastrasse 7, Osnabrueck, D 49069, Germany

Supporting Information

ABSTRACT:



Polycationic flexible pyridinium and rigid bipyridinium (=viologen) dendrimers were prepared. The cationic charges are persistent and equally distributed all through the dendrimers. The dendrimers are filled with monoanionic (benzenesulfonate (BS)), dianionic (anthraquinone disulfonate (AQDS), naphthalene disulfonate (NDS)), and trianionic (pyranine (Pyr)) guest molecules in a stepwise inside-out, shell-by-shell fashion. The total cationic charge per dendrimer subshell divided by the charge of a guest anion defines the maximum guest capacity of the corresponding shell. These numbers appear as “magic numbers” in ^1H NMR titrations. Thus, the proof for the sequential inside-out complexation scenario is based on the sequential appearance of the innermost, then the mid and finally the outermost dendrimer shell. Anions with matching size show the sharpest ^1H δ -transitions at the subshell equivalence points indicating that beside simple charge interaction molecular recognition is playing an important role. The end points of the generation 0 dendrimers were further probed by electrochemical techniques, yielding $K > 10 \times 10^3 \text{ M}^{-1}$ for the last guest molecule. Two reasons for the inside-out filling were identified from simple MM+ based MD calculations, i.e., (i) backfolding of outer branches leading to multiple complexation of anionic sites in all except the outermost shell, and (ii) the reduced mobility of the core region as compared to the outer branches leading to an enhancement of the cationic attractor over time and space in the central dendrimer region. The sequential inside-out filling of guest counterions within the dendrimers is in agreement with a wrapping process in combination with the observed decreasing hydrodynamic radius.

1. INTRODUCTION

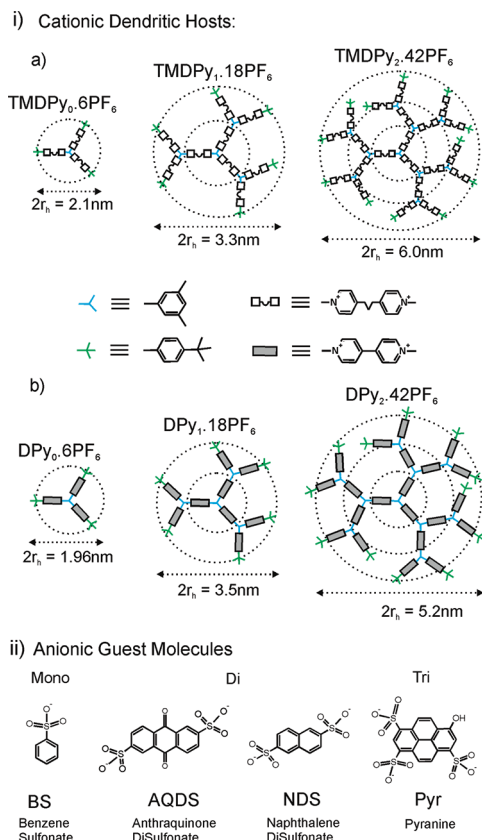
Dendrimers can act as hosts¹ for smaller molecular guests, a fact that has been used for fundamental studies^{2,3} as well as for drug delivery applications.^{4–8} Depending on the functionalities present on the dendrimer - ionic,^{9–15} neutral,¹⁶ hydrophobic,^{2,6} and H-bonding,^{2,17–21} guest molecules can be complexed and transported.²² The usual divergent synthetic procedures allow producing such functionalities exclusively at the core, along the branches or at the periphery, opening the design of localized complexation sites within a dendrimer.^{23–26} Beside active complexation, steric phenomena can determine the localization of molecular guests in a dendrimer, i.e., the voids in the innermost molecular shell of highly branched dendrimers appearing close to their limiting generation.¹ On the other hand there exist dendrimers with complexation sites (e.g., charges, Lewis base coordination sites) distributed all through the dendrimer (center, branches and periphery) equally. The PPI (polypropyleneimine), PAMAM (polyamidoamine), and poly(phenylazomethine), as well as pyridinium and viologen dendrimers are examples of such structures, and the question arises, if there

exists a preference for a substoichiometric amount of guest molecules to coordinate first in the center, at the branches or at the periphery of the dendrimer. So far there exist only two principal types of dendrimers with identical repeating subunits from the core into the periphery on which this question has been studied. These are (i) the phenylazomethine dendrimers with phenylimine based basic coordination sites for Sn^{2+} ,^{27–29} Fe^{3+} ,³⁰ ferrocenium,³¹ triphenylmethylm, ³¹ PtCl_4^{2-} ,^{31,32} and Ti^{4+} ,³³ all described by Yamamoto and co-workers, and (ii) a pyridinium dendrimer with equally distributed cationic sites binding anthraquinone disulfonate electrostatically.³⁴ Interestingly, in both types of hosts it was found that the dendrimers are filled with the corresponding guest molecules following a stepwise shell-by-shell mechanism starting with the innermost molecular shell and ending with the outermost shell. In the case of the phenylazomethine dendrimers, it was argued that a radial Lewis basicity gradient

Received: July 14, 2011

Revised: September 21, 2011

Published: October 11, 2011

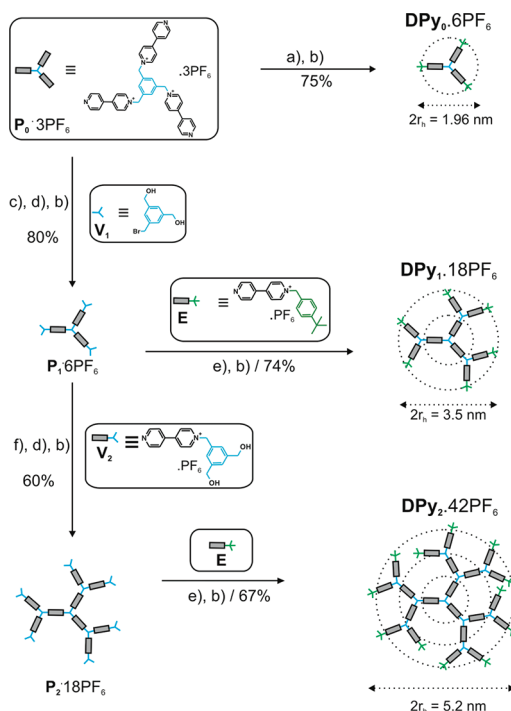
Scheme 1. Structure of Host and Guest Molecules^a

^a(i) Cationic dendritic hosts: (a) TMDPy_{0–2} dendrimers; (b) DPy_{0–2} dendrimers. (ii) Anionic guest molecules; r_h: hydrodynamic radii from DOSY.

within the dendrimer is responsible for this selectivity, and it was also shown that an electron withdrawing dendrimer core can invert the gradient leading to an outside-in filling mechanism.²⁸ Notably, there are several examples of dendrimers with tailored gradients consisting of branches with a continuously changing property, but most concern radial electron and photon flow rather than guest molecules. These dendrimers have a built-in redox gradient,^{10,32,35} or a built-in energy gradient.^{36,37}

A radial guest distribution can be synthetically provoked by a corresponding functionality gradient on the dendrimer branches. However, the inside-out scenario has also been observed without tailoring, using equally distributed identical functionalities on the dendrimer skeleton. Yamamoto has described this situation for a series of guests (cationic Lewis acids) together with phenylazomethine based dendrimers. We have found it for anthraquinone disulfonate and a dendrimer with equally distributed cationic pyridinium coordination sites. The reasons for this “dendritic effect” remain unclear.

Hence, we extended our studies using two classes of dendrimers one built from relatively rigid dicationic viologen subunits (DPy_{0–2}) and the other containing more flexible trimethylenedipyridinium subunits (TMDPy_{0–2}). They were probed with a series of anionic guest molecules (Scheme 1). For the viologen dendrimers efficient anion complexation and guest release has been reported by Balzani et al. but the mechanism of filling these

Scheme 2. Divergent Synthesis of Viologen Dendrimers with 4-*tert*-Butylbenzyl End Group^a

^aKey: (a) 4-*t*-Bu-BnBr/CH₃CN/80 °C; (b) NH₄PF₆/H₂O; (c) V₁/CH₃CN/80 °C; (d) HBr/HOAc/RT; (e) E/CH₃CN/80 °C, (f) V₂/CH₃CN/80 °C; dotted circles represent subshells r_h: hydrodynamic radii from DOSY

dendrimers was not addressed.³⁸ It has been shown that viologen dendrimers complexes DNA (polyanions with phosphate residues).³⁹ In the present work, we check the generality of the inside-out filling mechanisms with emphasis on the mutual fit of guest anions and host coordination sites. We include guest anions with one to three negative charges and we study the influence of the rigidity of the dendrimer structure. Finally, we try to rationalize the results by simulation of the coordination process using MD (molecular dynamics) calculations.

2. RESULTS AND DISCUSSION

a. Synthesis. The dendrimer structures and the guest anions used in the study are presented in Scheme 1.

The synthesis of the TMDPy_{0–2} series has been reported recently.³⁴ For the current study we have prepared the viologen dendrimers (DPy_{0–2}) with the same 4-*t*-BuBn peripheral groups rendering them sufficiently soluble in DMSO (dimethyl sulfoxide) (Scheme 2). The synthesis follows the general procedure as reported for viologen dendrimers with peripheral ethyl end groups.⁹ The intermediates V₁, V₂·PF₆ have been prepared as described,⁴⁰ synthesis and characterization of P₀·3PF₆, P₁·6PF₆ and P₂·18PF₆ is presented in the Experimental Section and in the Supporting Information.

The three peripheral nitrogens in P₀·3PF₆ react quantitatively with excess of 4-*t*-Bu-BnBr. Its reaction with P₀·3PF₆ followed by ion exchange yielded DPy₀·6PF₆ in 75%. The dendrimers DPy₁·18PF₆ and DPy₂·42PF₆ were available from the reaction of the corresponding precursors P₁·6PF₆ and P₂·18PF₆ with the

end group $E \cdot PF_6$, yielding 74 and 67%, respectively, after ion exchange. The intermediates and products were characterized by 1H NMR, ^{13}C NMR, and DEPT measurements. The purity of the compounds was further checked by elemental analysis (samples were pure apart from variable water contents). The completeness of N-alkylation was judged from the integration of the 1H NMR signals for the peripheral group as compared to the core resonances (For detailed synthetic procedures and characterization, see Supporting Information). The hydrodynamic radii of the dendrimers were measured by DOSY (diffusion ordered spectroscopy).

In the current paper, the complexation behavior of both series of dendrimers (DPy_{0-2} and $TMDPy_{0-2}$) was studied with mono-anionic (benzenesulfonate (BS)), dianionic (anthraquinone disulfonate (AQDS)) and naphthalene disulfonate (NDS)) and trianionic (pyranine (Pyr)) guest molecules. Both dendrimer series carry more or less equally distributed cationic charges which are arranged in molecular shells, i.e., 6, 12, and 24 pyridinium units for the second generation dendrimers. The interactions were monitored by 1H NMR technique. MM+ and MD simulations were performed to understand the radial affinity gradient.

b. Host–Guest Interactions— 1H NMR titrations. 1H NMR technique has been often used to evaluate the intermolecular interactions between host and guest in supramolecular assemblies, as even small differences in the chemical environment occurring upon complex formation can be detected.^{41–43} Guest interaction on dendrimers monitored by NMR techniques have been reported, e.g. the protonation of DAB (diaminobutane) and PAMAM (polyamidoamine) dendrimers by different acids (vitamin C, B_3 , and B_6) by Astruc et al.,¹⁷ or hydrogen bonding interactions in adamantyl-urea functionalized PPI dendrimers by Meijer et al.^{44,45} In the current case, host–guest complexation studies were carried out with DPy_{0-2} and $TMDPy_{0-2}$ dendrimers, and with benzenesulfonate (BS), naphthalene-2,6-disulfonate (NDS), anthraquinone-2,6-disulfonate (AQDS) and pyranine (Pyr) as guest molecules. The complexation progress was followed on host protons shifts.

1H NMR spectra of the $TMDPy_1$ and DPy_1 dendrimers dissolved as PF_6^- salts in $DMSO-d_6$ are presented in Figure 1. The corresponding spectra of $TMDPy_0$, DPy_0 , $TMDPy_2$, and DPy_2 are similar (see Supporting Information). The complete structural assignment of the protons within the repetitive sub-units is possible, but no subshell specific shifts are observed. The H_1 resonances on the pyridinium ($TMDPy$ and DPy) shows large splitting, whereas H_3 on the phenyl branching unit shows only minor splitting. This points to a preferential conformation of the methylene bearing H_5 rendering the two H_1 magnetically nonequivalent, but the three H_3 magnetically almost equivalent. The resonances due to meta- H_2 ($TMDPy$ and DPy) at pyridinium, as well as the protons at the trimethylene bridge [$TMDPy$ (H_6 and H_7)] show almost no splitting indicating reasonable rotational freedom of the bridge methylene groups before complexation. Since the region from δ 0.9 to 4 (trimethylene (in the case of $TMDPy$) and *t*-Bu end groups) is dominated by solvent peaks and tetrabutyl ammonium (counterion of the anionic guests), we focused mainly on the changes in the region δ 5.7–9.5.

Upon addition of guest anions the host protons H_1 , H_2 , H_3 , H_4 , and H_5 (pink circles in Figure 1) were splitting, indicating substantial interactions between host and guest. Because of interfering guest proton resonances it was not possible to monitor the whole set of indicator protons on the host for each guest molecule. Maximum splitting (0.1–0.4 ppm) were observed for H_1 , H_3 , and H_5 , and

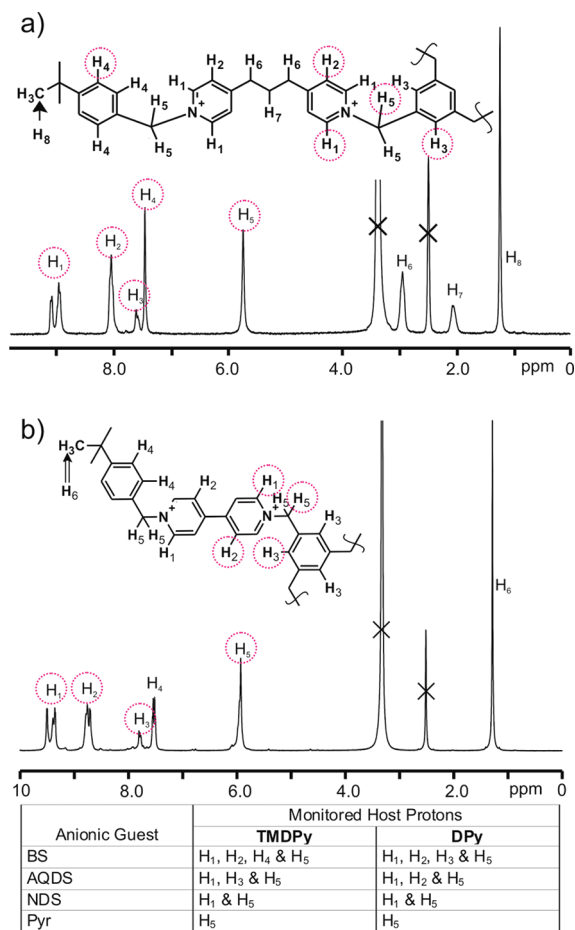


Figure 1. 1H NMR spectrum of (a) $TMDPy_1$ and (b) DPy_1 with chemical shift assignment. Dotted pink circles indicate the protons monitored during titration; the inset table shows the host protons monitored for different guests.

consistently smaller shifts (0.01–0.04 ppm) for H_2 and H_4 , and larger splitting on the host protons was observed for increasing size and charge on the guest molecules. Proton H_5 shows beside the splitting phenomenon peak broadening, possibly resulting from a short spin–spin relaxation time T_2 .^{46,47} The similarity of the splitting of the host proton resonances for different guest molecules (even though all flat and anionic) is astonishing. It points to similar locations of the anions within the host and to a similar freezing of the host conformational freedom. In spite of the obvious host–guest interaction, no host–guest $^1H, ^1H$ COSY (correlation spectroscopy) signals could be detected.

The following section concerns 1H NMR studies of the flexible $TMDPy_{0-2}$ and the rigid DPy_{0-2} dendrimers titrated with the different anions from the substoichiometric up to slight guest excess. It is organized according to the guest molecules, each of them interacting with generation 0–2 of the two dendrimer types. Assuming charge interaction as the main driving force, stoichiometric addition is defined as the point where equal amounts of charges from host and guest are present in the solution (charge ratio =1). For example, a dendrimer of generation 2 has 42 persistent positive charges, and thus 42 equiv of a guest with 1 negative charge, or 21 guest equivalents with 2 negative charges and so on are necessary for total charge compensation. Of importance for the following discussion is

Table 1. Theoretical Maximum Sub-Shell Capacities for Mono-, Di-, and Trianions

	gen. 0		gen. 1			gen. 2			
	ss 0	Σ	ss 0	ss 1	Σ	ss 0	ss 1	ss 2	Σ
A ⁻	6	6	6	12	18	6	12	24	42
A ²⁻	3	3	3	6	9	3	6	12	21
A ³⁻	2	2	2	4	6	2	4	8	14

the concept of subshells. A subshell (ss) is defined as the space occupied by bipyridinium moieties with identical number of bonds from the dendrimer center, i.e. a generation 0 dendrimer has a single ss, whereas generations 1 and 2 have 2 and 3 subshells, respectively. Theoretical maximum subshell capacities for mono-, di-, and trianionic guests (A⁻, A²⁻, A³⁻) in our dendrimers are as listed in Table 1.

The above-mentioned stoichiometric addition for total charge compensation corresponds to the sum of subshell capacities (Σ). In the framework of subshells, the inside-out filling of guest molecules (A) into a second generation dendrimer means that upon substoichiometric equivalent additions first subshell 0, then subshell 1 and finally subshell 2 (identical with end point titration) are filled. For an outside-in scenario the subshell filling sequence is reversed. The number of added equivalents for a change in subshell filling is represented in the following equations for dendrimers of generation 2 and guests with charge -1 to -3 :

$$\sum \text{inside-out for A}^{-} \quad 6 \rightarrow 18 \rightarrow 42 \quad (1)$$

$$\sum \text{outside-in for A}^{-} \quad 24 \rightarrow 36 \rightarrow 42 \quad (-1)$$

$$\sum \text{inside-out for A}^{2-} \quad 3 \rightarrow 9 \rightarrow 21 \quad (2)$$

$$\sum \text{outside-in for A}^{2-} \quad 12 \rightarrow 18 \rightarrow 21 \quad (-2)$$

$$\sum \text{inside-out for A}^{3-} \quad 2 \rightarrow 6 \rightarrow 14 \quad (3)$$

$$\sum \text{outside-in for A}^{3-} \quad 8 \rightarrow 12 \rightarrow 14 \quad (-3)$$

Generation 1 dendrimers shows the same pattern except that the last column is missing, and generation 0 dendrimers can obviously only give an end point. If there would be no preference for any subshell, i.e., assuming no gradient, the filling would be governed purely by probability, i.e., by the sites available in the different subshells as compared to the total amount of coordination sites. Intermediate cases governed by statistics and a gradient are also conceivable. Thus, the experimental problem is to find a spectroscopic method which discriminates filled and empty subshells during a titration experiment. This is done by looking at discontinuities in a plot of the spectroscopic observable vs added number of guest aliquots. In the studies of Yamamoto et al.,²⁹ it is the appearance of a new isosbestic point in UV/vis titration, and in our study, it is the appearance of a new ¹H NMR splitting distance (jump) or in some cases, a change of slope (δ vs guest conc.). In both studies completion of a subshell filling is related to the start/end and not the midpoint of the discontinuity in the titration.

We have called such discontinuities on the aliquot axis “magic numbers”. Even without knowing the physical background of the

spectral changes, it is obvious that “magic numbers” can eventually be interpreted within the theory of subshell occupancies (eq 1-2).

The experimental recognition of a discontinuity and its discriminative value with respect to the different filling scenarios is not straightforward. For the following we define discontinuities as the start of ¹H NMR peak splitting or a prominent change in the slope of host peak shifts upon guest addition. We use a triangle to indicate such a discontinuity in case of an end-point and circles in case of a filled subshell. Full lines are used if the discontinuity is well developed, dotted circles and triangles, if their identification is difficult. We stretch these symbols horizontally in order to include the exp. value and its interpretation (additive subshell capacity, end point) under the surface of the symbol. Thus, the weaker and broader a symbol appears, the weaker is its interpretative power. The interpretation of magic numbers as additive subshell capacities relies obviously on complete complex formation (no free guest), and on significant differences in subshell-specific association constants.

i. Interaction with AQDS. Selected ¹H NMR regions showing the host protons H₁, H₂/H₃ and H₅ for all 6 dendrimers **TMDPy**₀₋₂ and **DPy**₀₋₂ as a function of added dianionic AQDS equivalents are shown in Figure 2 (notably, the left panel in Figure 2 has been published earlier³⁴ and is shown here solely for the purpose of comparison). No precipitation is observed during the titration except above the point of total charge compensation, where haziness starts. For **TMDPy**₂, changes become small above full charge compensation, indicating an end point situation, whereas in case of **DPy**₀₋₂ spectral changes tend to continue after the theoretical end point. This may be related to a better fit of AQDS onto the host site, i.e., trimethylene-spaced bipyridinium in **TMDPy**₀₋₂ as compared to 4,4'-bipyridinium in **DPy**₀₋₂. Prominent changes occur at the same number of added equivalents AQDS independent of the dendrimer type and its generation, e.g. Three equiv AQDS added leads to splitting of H₅ in **TMDPy**₁ and **TMDPy**₂, or after 9 equiv added, collapse of the splitting of H₁ in **TMDPy**₁ and **TMDPy**₂ is observed. Thus, the “magic numbers” 3, 9, and 21 are read out for both dendrimer types with AQDS as a guest, which is consistent with an inside-out filling scenario (eq -1). Furthermore, addition of 3 equiv of AQDS to **TMDPy**₀ (end point) has a similar effect on H₁ and H₅ when added to **TMDPy**₁ and **TMDPy**₂ (subshell filling) or on H₅ for **DPy**₀₋₂ (black arrows). This behavior is a typical “inner most shell localized” response of protons.

ii. Interaction with NDS. NDS is dianionic as AQDS, but slightly smaller. A detailed study of the NMR shifts of the host protons H₁ and H₅ for all dendrimers **TMDPy**₀₋₂ and **DPy**₀₋₂ as a function of added dianionic NDS equivalents is shown in Figure 3. No precipitation is observed during the titration. Changes observed above full charge compensation are more pronounced as compared to AQDS, but still indicating an end point situation at least for **TMDPy**₀₋₂. H₅ discontinuities at subshell fillings are better structured in **DPy** as compared to the **TMDPy** dendrimers. Beside the above-discussed “inner most sub-shell response” a localized response from the second shell can be observed (magenta arrows). The observed “magic number” sequence 3, 9, 21 is read out and interpreted again as an inside-out filling mechanism, according to eq -1.

iii. Interaction with Monoanions. Trifluoromethanesulfonate (TFMS) and benzenesulfonate (BS) were chosen as monoanionic guest molecules and checked for their interaction with the dendrimers using the same technique (Figure 4). According to

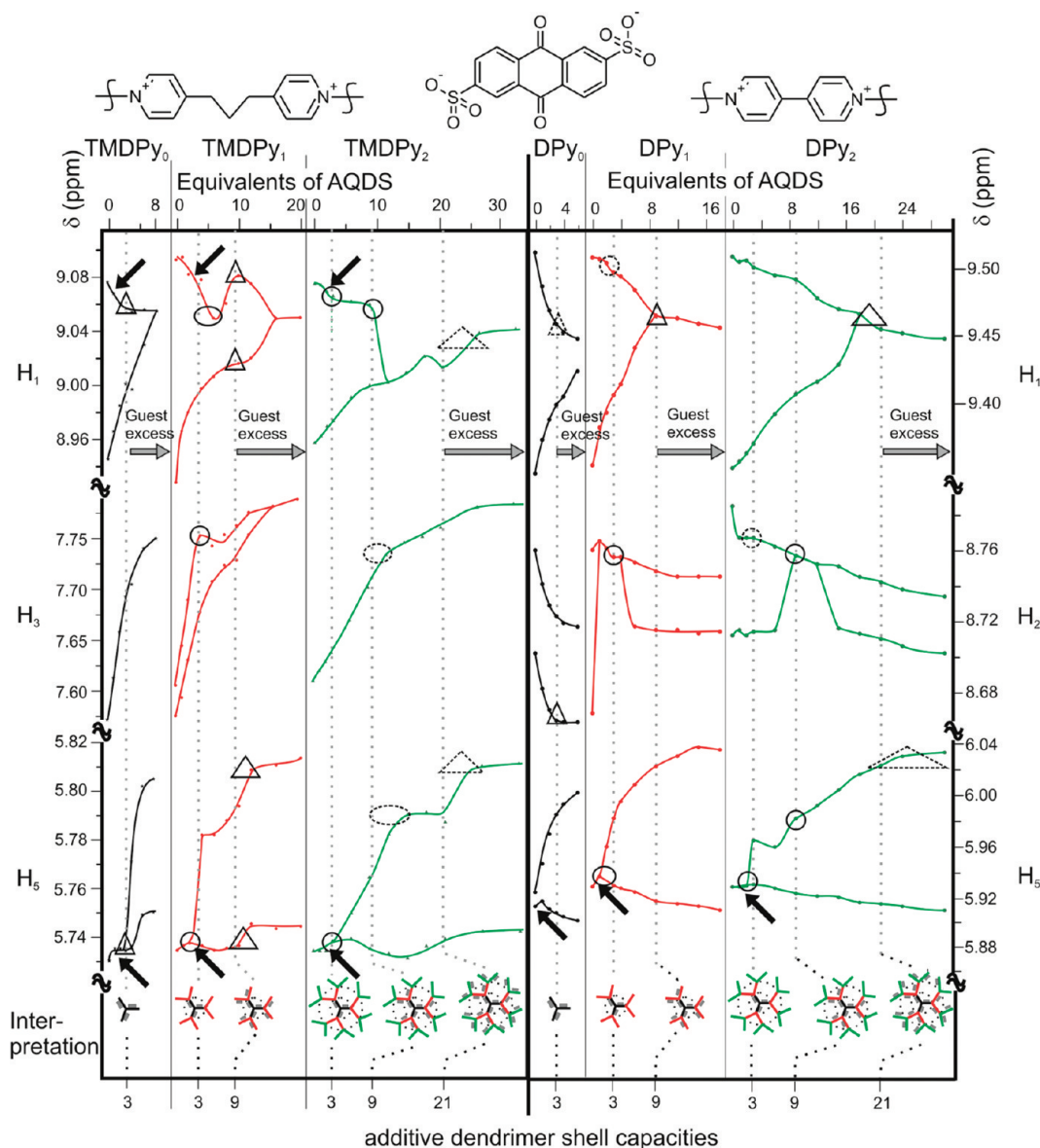


Figure 2. Plot of ^1H NMR peaks H_1 , H_3 and H_5 of TMDPy_{0-2} vs AQDS equivalent additions: $[\text{TMDPy}_0] = 3.2 \text{ mM}$; $[\text{TMDPy}_1] = 1.1 \text{ mM}$; $[\text{TMDPy}_2] = 0.48 \text{ mM}$ (left 3 columns) adapted from the literature,³⁴ and DPy_{0-2} vs AQDS equivalent additions; $[\text{DPy}_0] = 3.3 \text{ mM}$; $[\text{DPy}_1] = 1.2 \text{ mM}$; $[\text{DPy}_2] = 0.5 \text{ mM}$ (right 3 columns) in $\text{DMSO-}d_6$. Key: dotted lines, dendrimer subshell capacities; circles, subshell appearance; triangles, end point appearance; black arrows, innermost shell localized response.

eq 1 the magic numbers 6, 18, 42 are expected for the inside-out filling. TFMS additions do not affect the NMR spectrum of the dendrimers at all. The PF_6^- ion, which is present as a counterion in all dendrimers from the synthesis and the added TFMS do not interact closely with the dendrimer. Benzenesulfonate addition, on the other hand reveals that its interaction with the dendrimer is important (Figure 4). Less structured titration curves and smaller splitting distances are observed as compared to the two dianionic guests. In the case of TMDPy_{0-2} , prominent changes of the H_1 occur at or near the theoretical end points, whereas in the case of DPy_{0-2} end points are not easily identified (triangles, Figure 4). The innermost subshell appears as “magic number” 6 (mostly offset toward smaller aliquot concentrations) on most indicator protons in both dendrimer series (H_1 , H_2 and H_5 , circles in Figure 4). The second subshell changes are again subshell specific (magenta arrows) and manifest themselves mainly on the

H_5 resonance. This finding points to the same mechanism, i.e. the general inside-out filling.

iv. Interaction with Pyr. The titration curves of TMDPy and DPy dendrimers with the trianion pyranine are shown in Figure 5. According to eq 2 the “magic numbers” 2, 6, and 14 are expected for an inside-out filling mechanism. Only H_5 could be monitored because of interfering absorptions of the guest molecule, and unfortunately generation 2 precipitated above 8 equiv of guest addition. Splitting of H_5 is twice the amount observed for dianions. This is probably related to the increased conformational freezing of the dendrimer structure, as a single bipyridinium recognition site cannot account for total charge compensation of a trianionic guest requiring partial assistance of a second subunit. The end points in generation 0 and 1 are recognizable (the generation 2 end point was not measurable). Subshell filling is nicely reflected for the innermost shell in

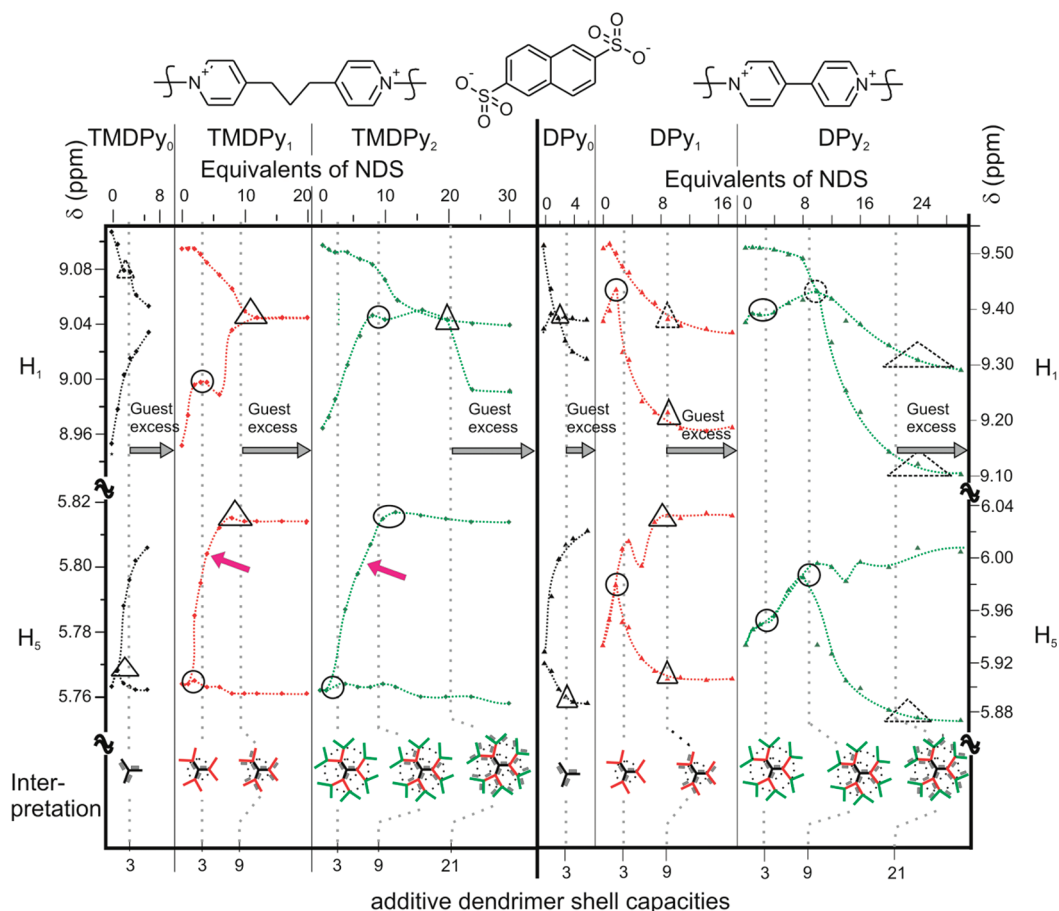


Figure 3. Plot of H_1 and H_5 dendrimer peaks of TMDPy_{0-2} vs NDS equivalent additions: $[\text{TMDPy}_0] = 3.2 \text{ mM}$; $[\text{TMDPy}_1] = 1.1 \text{ mM}$; $[\text{TMDPy}_2] = 0.48 \text{ mM}$; $[\text{DPy}_{0-2}]$ vs NDS equivalent additions; $[\text{DPy}_0] = 3.3 \text{ mM}$; $[\text{DPy}_1] = 1.2 \text{ mM}$; $[\text{DPy}_2] = 0.5 \text{ mM}$. Key: dotted lines, dendrimer shell capacities; circles, subshell appearance; triangles, end-point appearance; magenta arrows, second shell localized response.

generations 1 and 2, but the second subshell in the generation 2 dendrimers does not show up. The observed “magic number” 2 is still indicative for an inside-out filling mechanism (eq 2). However, as one of the reviewer mentions, the mutual fit of host and guest charges is less clear, and other filling scenarios can be envisaged.

The results of the titration experiments are summarized in Table 2. Notably, in the Table we represent the experimental subshell capacities in contrast to the additive subshell capacities (magic numbers).

In conclusion, the monoanion BS, the dianions AQDS and NDS, as well as the trianion Pyr show all more or less well-defined titration end points, except for some extension into the excess guest region. This happens mainly for guests which do not fit well onto the pyridinium coordination sites. An excellent mutual fit is observed between AQDS and the dicationic subunits in TMDPy_{0-2} . This is similar as the results of Balzani et al. using eosin²⁻ and DPy_{0-2} with different peripheral groups.¹² In contrast to their work based on fluorescence quenching, we are able to observe additionally the subshell filling. Subshell filling can be as sharp as the end point titration, and from the sequence of subshell capacities appearing in the titration we have established a general shell-by-shell inside-out filling mechanism for pyridinium based dendrimers and the anionic organic guests presented here.

c. Electrochemical End Point Titrations. Different host–guest interactions observed in the preceding paragraph by ¹H

NMR titration have further been probed by electrochemical methods. In Figure 6, the cyclic voltammograms (CVs) of the nonelectroactive TMDPy_0 (0.5 mM) in DMSO/0.1 M TBA.PF₆ with 1–6 equiv electroactive AQDS (1 equiv = 0.17 mM, corresponding to 1 of 3 available coordination sites in TMDPy_0) are represented. Free and complexed AQDS deliver different oxidation peaks, the complexed AQDS showing a retarded oxidation (slow electron transfer). The anodic peak currents of complexed and free AQDS are representative for their respective concentrations. If the peak currents are plotted against the equivalents of added AQDS (Figure 7.II), a well-defined end point of 3 can be read. The slight deviations from the extrapolated dotted and dashed lines indicate ca. 90% complexation for the third guest molecule (eq –2).

$$K_3^{0/0} = \frac{[\text{TMDPy} - \text{AQDS}_3]}{[\text{TMDPy} - \text{AQDS}_2] \times [\text{AQDS}]}$$

$$= \frac{0.45 \times 10^{-3}}{0.05 \times 10^{-3} \times 0.05 \times 10^{-3}} = 18 \times 10^3 \text{ M}^{-1}$$

Using the concentrations defined in Figure 6 and assuming 90% complexation a value of $K_3^{0/0} = 18 \times 10^3 \text{ M}^{-1}$ results (for further information on K values see Supporting Information). Notably, $K_3^{0/0}$ is the association constant for the third and last guest molecule pick-up of the generation 0 dendrimer and the Coulombic interaction is only 2 plus/2 minus. The association

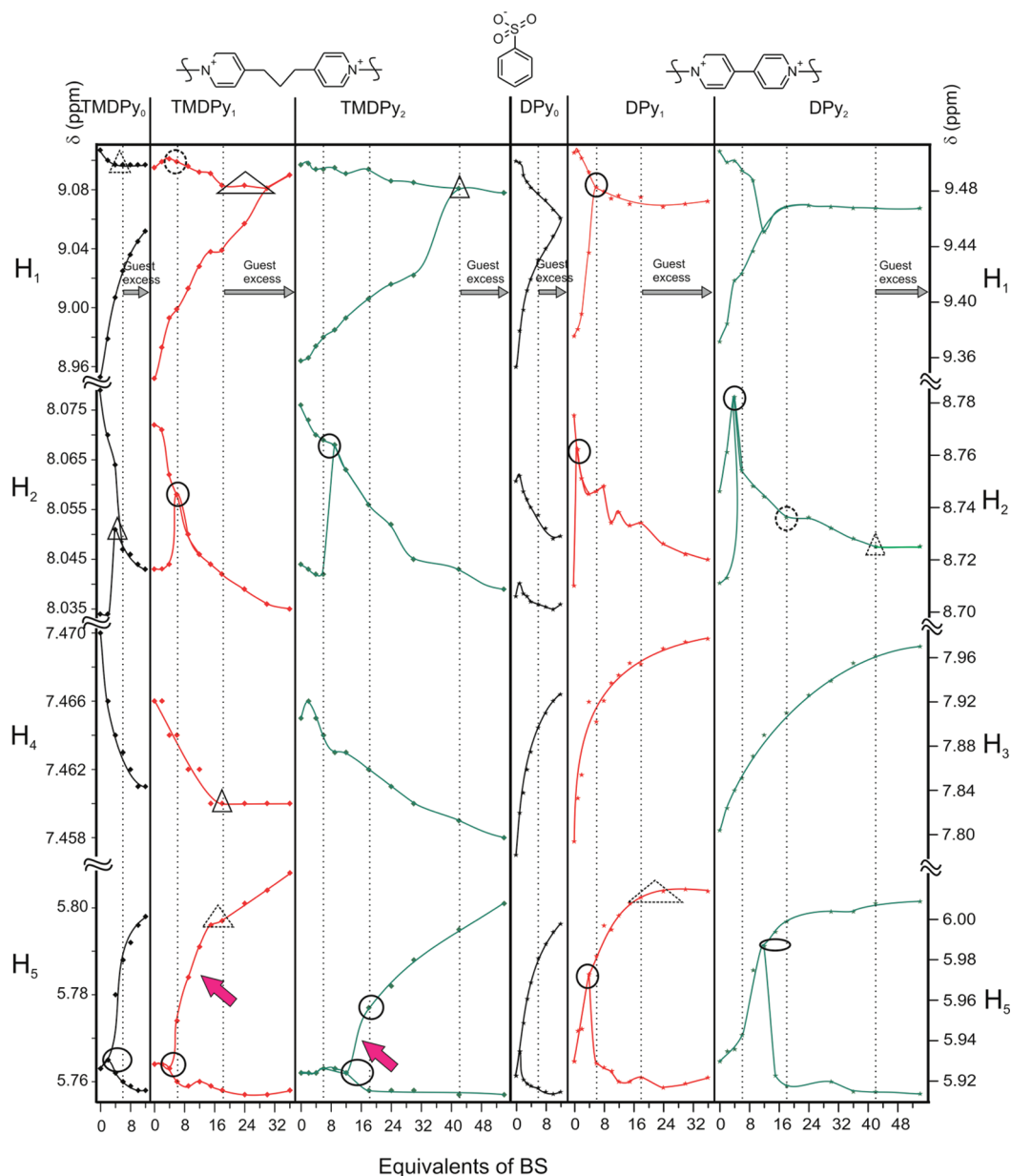


Figure 4. Plot of H_1 , H_2 , H_3/H_4 , and H_5 ^1H NMR peaks (TMDPy_{0-2} and DPy_{0-2}) vs benzenesulfonate (BS) addition: $[\text{TMDPy}_0] = 3.2$ mM; $[\text{TMDPy}_1] = 1.1$ mM; $[\text{TMDPy}_2] = 0.48$ mM; $[\text{DPy}_0] = 3.3$ mM; $[\text{DPy}_1] = 1.2$ mM; $[\text{DPy}_2] = 0.5$ mM. Key: dotted lines, dendrimer subshell capacities; triangle, end point; circles, subshell fillings.

constants for the first and second AQDS ($K_1^{0/0}$ and $K_2^{0/0}$) are therefore supposed to be larger (see peak current growth for the first and second addition indicating stoichiometric complexation). From the same reasoning the higher generation dendrimers are expected to have even larger association constants. Changing the electrolyte concentration (tetrabutylammonium hexafluorophosphate) in the range from 0.025 to 0.2 M has only a minor effect on the association constants (not shown), indicating that PF_6^- has an association constant orders of magnitude smaller.

The electroactive dendrimer DPy_0 was titrated with the nonelectroactive NDS yielding a minor but reproducible jump of the first formal reduction potential (E^0) for the first, second and third guest molecules, i.e., up to the stoichiometric amount is observed (Figure 7). The same behavior is observed

on the second reduction of the dendrimer (not shown). The phenomenon could be related to the expulsion of NDS upon reduction of the host.

If the amount of NDS is further increased, E^0 decreases steadily (ca. 10 mV per decade, its origin is not clear). As the fourth addition is sitting on the dotted line in Figure 7, we assume again complete association with three guest molecules present. An accurate quantification of the $K_3^{0/0}$ value is not possible, but its minimum value is $>10 \times 10^3 \text{ M}^{-1}$.

d. Molecular Modeling. The observed inside-out guest filling scenario is astonishing. Molecular dynamics calculations (using the MM+ force field) were carried out to shine light on the background of this mechanism.

Force field modeling MM+ implemented on Hyperchem 8.08⁴⁸ was used to judge the structure and size of the dendrimers as a

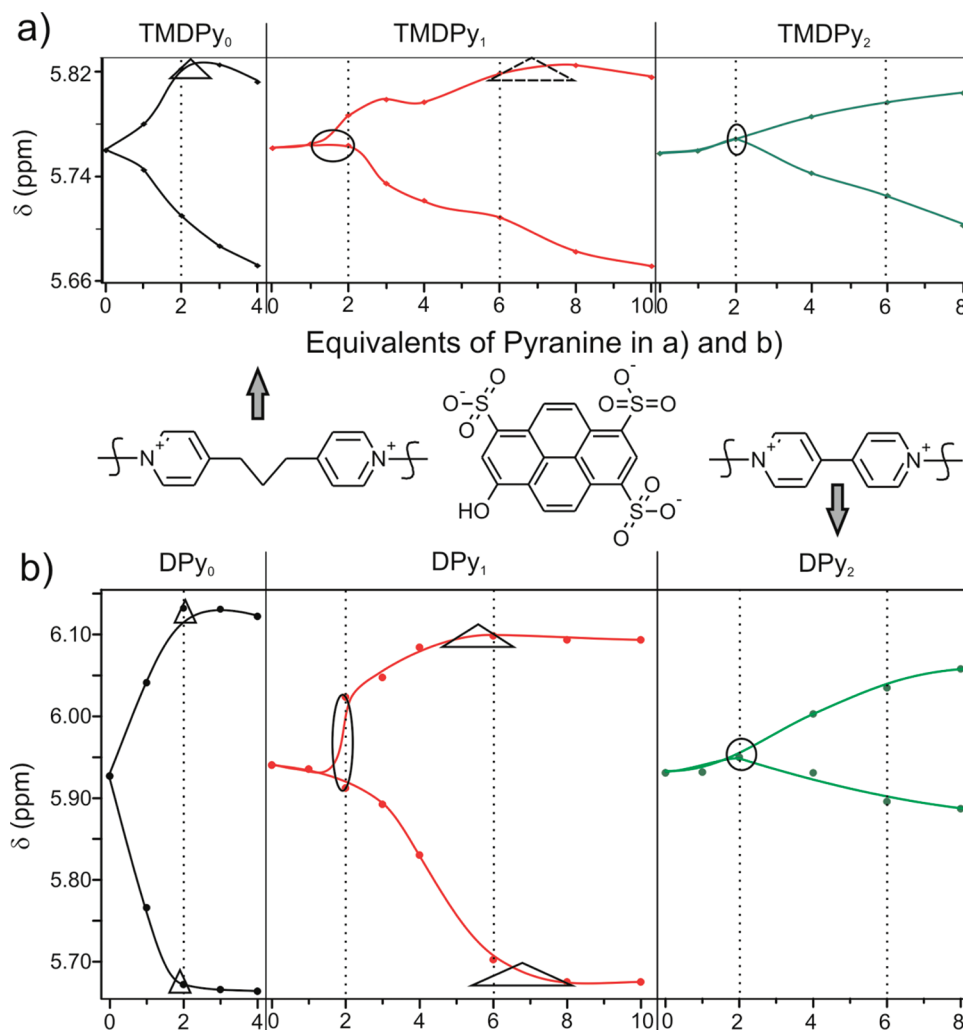


Figure 5. Plot of H_5 1H NMR-peak of TMDPy (a) and DPy (b) dendrimers vs added Pyr equivalents: $[TMDPy_0] = 3.2$ mM; $[TMDPy_1] = 1.1$ mM; $[TMDPy_2] = 0.48$ mM; $[DPy_0] = 3.3$ mM; $[DPy_1] = 1.2$ mM; $[DPy_2] = 0.5$ mM in $DMSO-d_6$. Key: dotted lines, dendrimer subshell capacities; black circles, appearance of $ss(0)$ in generation 2.

Table 2. Observed and Theoretical Sub-Shell Capacities

hosts	no. of guest anions in the 1st 2nd 3rd dendrimer subshell ^a							
	monoanion		dianions				trianion	
	BS		NDS		AQDS		Pyr	
	exp. observed ^d	model	exp. observed ^d	model	exp. observed ^d	model	exp. observed ^d	model
DPy ₀	~6–9 ^c	6	2–3 ^c	3	3 ^c	3	2	2
DPy ₁	~4–6 ~12	6 12	3 6	3 6	3 6 ^c	3 6	2 3–5	2 4
DPy ₂	~5 ~12 ~	6 12 24	3 6 ~12 ^c	3 6 12	~2 ~6 ~12 ^c	3 6 12	2 ^b	2 4 8
TMDPy ₀	4–6 ^c	6	2–3	3	3 ^c	3	2–3	2
TMDPy ₁	~6 ~12 ^c	6 12	2–3 ~6	3 6	~3 6–8 ^c	3 6	2 4–5	2 4
TMDPy ₂	~6 1–2 24	6 12 24	2–3 6 12	3 6 12	3 6–8 ~12	3 6 12	2 ^b	2 4 8

^a Individual subshell capacities, in contrast to eq 1–2, where additive subshell capacities are used. ^b Precipitation. ^c Guest excess. ^d Interpretation of results in Figure 2-5

function of the generation before and after guest complexation. MD calculations were used with the same force field to visualize

the pick-up of the anionic guest molecules and the final localization of the guest molecules within the subshells. Notably, these are gas

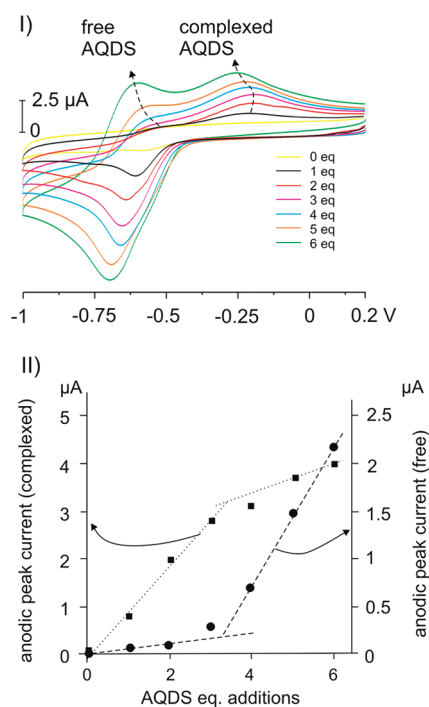


Figure 6. (I) Cyclic voltammetry (CV) of nonelectroactive TMDPy_0 (2.5×10^{-6} mol, 0.5 mM) in DMSO/0.1 M TBA.PF₆ with 1–6 equiv electroactive AQDS (1 equiv = 0.83×10^{-6} mol = 2.5×10^{-6} /3 mol = 1 site of 3 available in TMDPy_0); CVs showing oxidation of free and TMDPy_0 -complexed AQDS at different potentials. (II) Analysis of the peak currents of free (circles) and complexed AQDS (squares) vs AQDS-additions yielding ca. 90% complexation for 3 AQDS added.

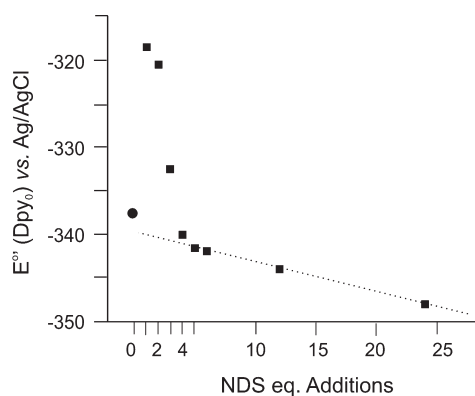


Figure 7. Formal reduction potential (E^0) from CV's (not shown) of electroactive DPy_0 (2.5×10^{-6} mol, 0.5 mM) in DMSO/0.1 M TBA.PF₆ with 1–24 equiv nonelectroactive NDS (1 equiv = 0.83×10^{-6} mol = 2.5×10^{-6} /3 mol = 1 site of 3 available in DPy_0).

phase calculation neglecting solvent and counterions and therefore the charge interaction (each pyridinium site carries +1, and each sulfonate oxygen -0.33), a fact that was counterbalanced by relatively high bath temperatures during MD equilibration. More sophisticated MD calculations on the guest location within a dendrimer are known, but they do not concern electrostatic binding.⁴⁹ In the absence of counterions our dendrimers extend their branches as far as possible from each other because of the repulsive charge interaction of the naked pyridinium sites. Non-dissociated counterions and a polar solvent would shield the

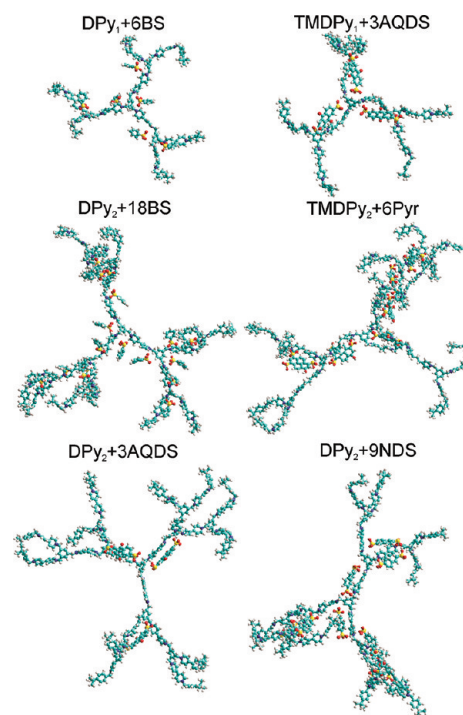


Figure 8. Equilibrated situations from MM+ MD calculations on TMDPy_{1-2} and DPy_{1-2} in the presence of selected guest anions.

cations and reduce this effect under experimental conditions, but an open structure is still ensured.⁵⁰

The generation 0 dendrimers adopt a flat disk structure, whereas generation 1 and especially 2 have dumbbell structure, all of them displaying an open architecture ensuring free access for a guest molecule at any pyridinium site (in contrast to higher generation PAMAM dendrimers with only partial protonation⁵¹). The approximate radii of the long axis of the ellipsoids together with those calculated from the exp. diffusion coefficients from DOSY experiments are in the Supporting Information. We have shown earlier that TMDPy_{0-2} contract upon addition of AQDS using DOSY. Unfortunately with the new systems described here, such measurements were not possible, because of large fluctuation in the diffusion coefficient values leading to large error margins (not reproducible). Upon addition of guest anions outside of the dendrimer periphery “in silico” the anions move toward the dendrimer obviously driven by the long-range electrostatic field established by the many point charges on the pyridinium ions. The first contact with a pyridinium charge is not necessarily their final destination. If the bathing temperature is high enough, they start generally to walk along the side chains toward the center of the dendrimer until they find their final place usually at the innermost free site. Upon stepwise addition of aliquots and waiting for the thermalized situation allows us to simulate the titration curve. The mono- or dianions are generally first filling the innermost coordination sphere, and then the second and third. It is astonishing to observe that in many cases our experimental results are 1:1 mimicked by the calculations. This is represented in Figure 8 by the end situations of MD calculations with different dendrimer types, and different generations in combination with different anions. The detailed analyses, as well as the 12 movies showing the complete approach and final complexation are available in the Supporting Information.

Complexation in the outermost coordination shell is probably less efficient (i) because there is no additional positive charge in a next outer shell that can fold back to complex a negatively charged guest in the next inner shell,³⁴ (ii) because of steric hindrance induced by the peripheral *t*-Bu group, and (iii) the electrostatic attractor in the center is stronger than in the branches or in the periphery. The latter can be explained by the larger motional freedom of the dendrimer subunits in the periphery as compared to those close to the center. Identical dendrimer subunits in the center move slower than in the periphery because of the different inertial masses involved. The corresponding pyridinium charges are therefore well localized over time in the center of the dendrimer, whereas they are smeared over space and time in the periphery. This phenomenon results in a stronger electrostatic attractor in the center of the dendrimer. Definitely, this is only fulfilled at generations far below the limiting dendrimer generation. Back-folding of outer branches onto an inner guest, and thereby favoring the inside-out mechanism, is also mainly in case of an open structure conceivable. Backfolding was observed during simulation and persists in the equilibrated situation; and it was detected experimentally from an increase of the diffusion coefficient upon small counterion addition. Further anion additions reopen the back folded branches as observed in silico and experimentally.³⁴

3. CONCLUSIONS

Flexible and rigid pyridinium dendrimers are sequentially complexed with 4 different types of mono-, di- and trianionic guest molecules in a stepwise inside-out, shell-by-shell fashion. The proof is based on the sequential appearance of the subshell capacities in NMR titrations. Anions with matching symmetry show more or less sharp transitions (δ , ppm) of the ¹H chemical shift at the end point and at subshell fillings. The same finding was reported earlier by Yamamoto for a very different dendrimer but also equally distributed coordination sites.²⁹

The same “inside-out” filling scenario was also found by gas phase MM+ MD calculations, pointing to a simple reason behind the phenomenon. Backfolding of outer branches and electrostatic attractors pointing toward the center of the dendrimer were visually identified. The central attractors develop because the charges in the periphery are in fast motion and therefore smeared as compared to the charges in the center.

Besides their theoretical impact, our findings open a way to fill a dendrimer shell-by-shell inside-out with different guests. Theoretically, one could sequentially complex different guest molecules and try to irreversibly fix them in a second step, creating a radial chemical gradient within a dendrimer that was originally seemingly without any gradient.

■ EXPERIMENTAL SECTION

Materials. All starting materials and solvents were purchased from Sigma-Aldrich and used without further purification. All reactions were performed under dry conditions. For the host–guest interaction studies, commercially available Benzenesulfonic acid sodium salt (BS), Anthraquinone-2,6-disulfonic acid disodium salt (AQDS), Naphthalene-2,6-disulfonic acid disodium salt (NDS) and pyranine trisodium salt (Pyr), DMSO-*d*₆ were ion-exchanged using TBA·Br in DCM/H₂O and the obtained tetrabutylammonium derivatives were NMR pure [slight excess of TBA·Br was noticed].

Characterization and Measurements. ¹H NMR, ¹³C NMR, and DEPT spectra were recorded on Bruker 250/500 Avance spectrometer at

25 °C using CD₃CN or DMSO-*d*₆ as a solvent and internal reference. All chemical shifts are reported in parts per million (δ , ppm) with respect to the internal standard. DOSY spectra were recorded on a Bruker Avance III 500 MHz spectrometer at 25 °C using DMSO-*d*₆ as a solvent. Diffusion measurements were performed using a ¹H NMR pulsed-gradient experiment: the simulated spin–echo sequence which leads to the measurement of the diffusion coefficient *D*, where *D* is the slope of the straight line obtained when ln(*I*) is displayed against the gradient-pulse power's square according to the following equation: $\ln(I) = -\gamma^2 G^2 D \delta^2 (\Delta - \delta/3)$, where *I* is the relative intensity of a chosen resonance, γ is the proton gyromagnetic ratio, Δ is the intergradient delay (60 ms), δ is the gradient pulse duration (varied between 1.5 to 5 ms), and *G* is the gradient intensity.

Elemental analyses were performed on Elementar Vario Micro cube instrument.

Electrochemical Titrations. Cyclic voltammetry was carried out at room temperature in a standard three-electrode cell using DMSO/0.1 M tetrabutyl ammonium hexafluorophosphate as solvent/electrolyte. The working electrodes were a glassy carbon disk (area = 0.066 cm², Metrohm 6.0804.010) and the counter electrode was a Pt wire. The reference electrode was a Ag/AgCl/KCl (3 M) electrode (Metrohm, 6.0724.140) separated by a salt bridge containing DMSO/0.1 M tetrabutyl ammonium hexafluorophosphate. Prior to each experiment, the working electrode was carefully polished with alumina powder and rinsed with distilled water. Potentiostatic control was provided by a PGSTAT 20 potentiostat from AUTOLAB connected to the cell and controlled by a PC running under GPES for Windows, Version 4.2 (ECO Chemie 1995). Formal potentials ($E^{0'}$) were calculated from cathodic and anodic peak potentials in CV's according to $E^{0'} = (E_{pc} + E_{pa})/2$. The scan rate was 100 mV/s.

¹H NMR Titration. The titration was carried out on a Bruker 250/500 MHz spectrometer in DMSO-*d*₆ by using a solution of dendrimer ([TMDPy/DPy] = 0.4–3.3 mM) at 298 K and adding aliquots of the anion which was more concentrated than the host solution. The concentration of the dendrimer remained constant throughout the experiment.

Synthetic Procedures. *Synthesis of 1-(4-tert-Butylbenzyl)-4-(pyridin-4-yl)pyridinium Hexafluorophosphate (E·PF₆).* 4,4'-Bipyridine (1.72 g, 11 mmol) and 4-tert-butylbenzyl bromide (1 g, 4.4 mmol) were dissolved in 50 mL DCM, refluxed for 2 h. The obtained yellow precipitate was filtered, washed with DCM and dried. The yellow solid thus obtained is dissolved in minimal quantity of water, precipitated with 3 M NH₄PF₆, filtered, washed with water and dried to yield 1-(4-tert-butylbenzyl)-4-(pyridin-4-yl)pyridinium hexafluorophosphate as a pale white powder (1.65 g, 84%). ¹H NMR (250 MHz, CD₃CN): δ , ppm 8.87 (s, 4H), 8.33 (s, 2H), 7.79 (s, 2H), 7.50 (dd, 4H), 5.74 (s, 2H), 1.34 (s, 9H). ¹³C NMR (63 MHz, CD₃CN): δ , ppm 154.5, 153.3, 151.1, 144.8, 141.2, 130.1, 128.9, 126.5, 126.3, 121.9, 63.9, 34.4, 30.4. Anal. Calcd for C₂₁H₂₃F₆N₂P: C, 56.25; H, 5.17; N, 6.25. Found C, 55.89; H, 5.16; N, 6.21.

DPy₀·6PF₆. P₀·3PF₆ (0.2 g, 195 μ mol) and 4-tert-butylbenzyl bromide (0.27 g, 1.2 mmol) were dissolved in 20 mL of CH₃CN, and the mixture was stirred at 80 °C for 2 d. The solution was cooled, filtered, washed with CH₃CN and dried. It was then dissolved in MeOH:H₂O (1:1) mixture, precipitated with 3 M NH₄PF₆, filtered, washed and dried to yield DPy₀·6PF₆ as a pale yellow powder (0.28 g, 75%). ¹H NMR (500 MHz, DMSO-*d*₆): δ , ppm 9.50 (d, J(H,H) = 6.5 Hz, 6H), 9.35 (d, J(H,H) = 6 Hz, 6H), 8.75 (d, J(H,H) = 7 Hz, 6H), 8.71 (d, J(H,H) = 6.5 Hz, 6H), 7.78 (s, 3H), 7.53 (dd, 12H), 5.92 (s, 12H), 1.28 (s, 27H). ¹³C NMR (125 MHz, DMSO-*d*₆): δ , ppm 152.8, 150.1, 149.3, 146.4, 146.2, 135.9, 131.6, 131.2, 129.2, 127.6, 127.5, 126.6, 63.9, 63.2, 34.9, 31.4. Anal. Calcd for C₇₂H₇₈F₃₆N₆P₆·3H₂O: C, 44.32; H, 4.34; N, 4.31. Found C, 44.35; H, 4.36; N, 4.39.

$DPy_1 \cdot 18PF_6$, $P_1 \cdot 6PF_6$ (0.15 g, 65 μmol) and $E \cdot PF_6$ (0.22 g, 492 μmol) were dissolved in 50 mL of CH_3CN , and the mixture was stirred at 80 °C for 4 d. The solution was cooled, filtered, washed with CH_3CN and dried. It was then dissolved in $\text{MeOH}:\text{H}_2\text{O}$ (1:1) mixture, precipitated with 3 M NH_4PF_6 , filtered, washed and dried to yield $DPy_1 \cdot 18PF_6$ as a pale yellow powder (0.26 g, 74%). ^1H NMR (500 MHz, $\text{DMSO}-d_6$) δ ppm 9.45 (m, 36H), 8.73 (m, 36H), 7.79 (m, 12H), 7.53 (dd, 24H), 5.93 (s, 36H), 1.28 (s, 54H). ^{13}C NMR (125 MHz, $\text{DMSO}-d_6$) δ ppm 152.8, 150.1, 149.4, 146.4, 146.2, 135.8, 131.2, 129.2, 127.6, 127.5, 126.6, 63.9, 63.2, 34.9, 31.4. Anal. Calcd for $\text{C}_{192}\text{H}_{198}\text{F}_{108}\text{N}_{18}\text{P}_{18} \cdot 9\text{H}_2\text{O}$: C, 41.71; H, 3.93; N, 4.56. Found C, 41.64; H, 3.80; N, 4.49.

$DPy_2 \cdot 42PF_6$, $P_2 \cdot 18PF_6$ (0.2 g, 32 μmol) and $E \cdot PF_6$ (0.20 g, 455 μmol) were dissolved in 50 mL CH_3CN , stirred at 80 °C for 4 d. The solution was cooled, filtered, washed with CH_3CN and dried. It was then dissolved in $\text{MeOH}:\text{H}_2\text{O}$ (1:1) mixture, precipitated with 3 M NH_4PF_6 , filtered, washed and dried to yield $DPy_2 \cdot 42PF_6$ as a pale yellow powder (0.27 g, 67%). ^1H NMR (500 MHz, $\text{DMSO}-d_6$) δ ppm 9.44 (m, 84H), 8.74 (m, 84H), 7.80 (m, 30H), 7.53 (dd, 48H), 5.93 (s, 84H), 1.28 (s, 108H); ^{13}C NMR (125 MHz, $\text{DMSO}-d_6$) δ ppm 152.8, 150.1, 149.7, 149.4, 146.6, 146.4, 146.2, 135.8, 131.6, 131.2, 129.2, 127.6, 127.5, 126.6, 63.9, 63.3, 34.9, 31.4; Anal. Calcd for $\text{C}_{432}\text{H}_{438}\text{F}_{252}\text{N}_{42}\text{P}_{42} \cdot 21\text{H}_2\text{O}$: C, 40.90; H, 3.81; N, 4.64. Found C, 40.77; H, 3.91; N, 4.53.

ASSOCIATED CONTENT

S Supporting Information. Text giving synthetic procedures of the intermediates, spectroscopic and analytical data for the intermediates, a table summarizing the physical parameters, MM+ simulations with start and end situations, 12 movies showing simulated complexations, and figures showing ^1H , ^{13}C and DEPT spectra. This material is available free of charge via the Internet at <http://pubs.acs.org>.

AUTHOR INFORMATION

Corresponding Author

*E-mail: Lowalder@uos.de.

ACKNOWLEDGMENT

M.K. thanks Graduate College 612 funded by the DFG and University of Osnabrueck for financial assistance.

REFERENCES

- Jansen, J. F. G. A.; de Brabander van den Berg, E. M. M.; Meijer, E. W. *Science (Washington, D.C.)* **1994**, *266*, 1226.
- Hu, J.; Cheng, Y.; Wu, Q.; Zhao, L.; Xu, T. *J. Phys. Chem. B* **2009**, *113*, 10650.
- Cheng, Y.; Wu, Q.; Li, Y.; Xu, T. *J. Phys. Chem. B* **2008**, *112*, 8884.
- Boas, U.; Heegaard, P. M. H. *Chem. Soc. Rev.* **2004**, *33*, 43.
- Gillies, E. R.; Frechet, J. M. J. *Drug Discovery Today* **2005**, *10*, 35.
- Morgan, M. T.; Carnahan, M. A.; Immoos, C. E.; Ribeiro, A. A.; Finkelstein, S.; Lee, S. J.; Grinstaff, M. W. *J. Am. Chem. Soc.* **2003**, *125*, 15485.
- Bosman, A. W.; Janssen, H. M.; Meijer, E. W. *Chem. Rev. (Washington, D.C.)* **1999**, *99*, 1665.
- Stiriba, S.-E.; Frey, H.; Haag, R. *Angew. Chem., Int. Ed.* **2002**, *41*, 1329.
- Heinen, S.; Walder, L. *Angew. Chem., Int. Ed.* **2000**, *39*, 806.
- Heinen, S.; Meyer, W.; Walder, L. *J. Electroanal. Chem.* **2001**, *498*, 34.
- Marchioni, F.; Venturi, M.; Ceroni, P.; Balzani, V.; Belohradsky, M.; Elizarov, A. M.; Tseng, H. R.; Stoddart, L. F. *Chem.—Eur. J.* **2004**, *10*, 6361.
- Stoddart, J. F.; Ronconi, C. M.; Balzani, V.; Baroncini, M.; Ceroni, P.; Giansante, C.; Venturi, M. *Chem.—Eur. J.* **2008**, *14*, 8365.
- Therien-Aubin, H.; Zhu, X. X.; Moorefield, C. N.; Kotta, K.; Newkome, G. R. *Macromolecules* **2007**, *40*, 3644.
- Boisselier, E.; Ornelas, C.; Pianet, I.; Aranzaes, J. R.; Astruc, D. *Chem.—Eur. J.* **2008**, *14*, 5577.
- Ornelas, C.; Boisselier, E.; Martinez, V.; Pianet, I.; Ruiz Aranzaes, J.; Astruc, D. *Chem. Commun.* **2007**, 5093.
- Morara, A. D.; McCarley, R. L. *Org. Lett.* **2006**, *8*, 1999.
- Boisselier, E.; Liang, L.; Dalko-Csiba, M.; Ruiz, J.; Astruc, D. *Chem.—Eur. J.* **2010**, *16*, 6056.
- Cooke, G.; Sindelar, V.; Rotello, V. M. *Chem. Commun.* **2003**, 752.
- Subramani, C.; Yesilbag, G.; Jordan, B. J.; Li, X.; Khorasani, A.; Cooke, G.; Sanyal, A.; Rotello, V. M. *Chem. Commun. (Cambridge, U.K.)* **2010**, *46*, 2067.
- Grimm, F.; Hartnagel, K.; Wessendorf, F.; Hirsch, A. *Chem. Commun.* **2009**, 1331.
- Zimmerman, S. C.; Wang, Y.; Bharathi, P.; Moore, J. S. *J. Am. Chem. Soc.* **1998**, *120*, 2172.
- Menjoge, A. R.; Kannan, R. M.; Tomalia, D. A. *Drug Discovery Today* **2010**, *15*, 171.
- Hourani, R.; Kakkar, A. *Macromol. Rapid Commun.* **2010**, *31*, 947.
- Boas, U.; Christensen, J. B.; Heegaard, P. M. H. *J. Mater. Chem.* **2006**, *16*, 3785.
- Hecht, S. J. *Polym. Sci., Part A: Polym. Chem.* **2003**, *41*, 1047.
- Posocco, P.; Ferrone, M.; Fermeglia, M.; Pricl, S. *Macromolecules* **2007**, *40*, 2257.
- Imaoka, T.; Tanaka, R.; Arimoto, S.; Sakai, M.; Fujii, M.; Yamamoto, K. *J. Am. Chem. Soc.* **2005**, *127*, 13896.
- Higuchi, M.; Tsuruta, M.; Chiba, H.; Shiki, S.; Yamamoto, K. *J. Am. Chem. Soc.* **2003**, *125*, 9988.
- Yamamoto, K.; Higuchi, M.; Shiki, S.; Tsuruta, M.; Chiba, H. *Nature* **2002**, *415*, 509.
- Nakajima, R.; Tsuruta, M.; Higuchi, M.; Yamamoto, K. *J. Am. Chem. Soc.* **2004**, *126*, 1630.
- Ochi, Y.; Fujii, A.; Nakajima, R.; Yamamoto, K. *Macromolecules* **2010**, *43*, 6570.
- Albrecht, K.; Yamamoto, K. *J. Am. Chem. Soc.* **2009**, *131*, 2244.
- Nakashima, T.; Satoh, N.; Albrecht, K.; Yamamoto, K. *Chem. Mater.* **2008**, *20*, 2538.
- Kathiresan, M.; Walder, L. *Macromolecules* **2010**, *43*, 9248.
- Selby, T. D.; Blackstock, S. C. *J. Am. Chem. Soc.* **1998**, *120*, 12155.
- Devadoss, C.; Bharathi, P.; Moore, J. S. *J. Am. Chem. Soc.* **1996**, *118*, 9635.
- Jiang, D. L.; Aida, T. *Nature* **1997**, *388*, 454.
- Marchioni, F.; Venturi, M.; Credi, A.; Balzani, V.; Belohradsky, M.; Elizarov, A. M.; Tseng, H. R.; Stoddart, J. F. *J. Am. Chem. Soc.* **2004**, *126*, 568.
- Bongard, D.; Bohr, W. (Germany). Application: DE DE, 2008; 10 pp.
- Kathiresan, M.; Walder, L.; Ye, F.; Reuter, H. *Tetrahedron Lett.* **2010**, *51*, 2188.
- Broeren, M. A. C.; de Waal, B. F. M.; van Genderen, M. H. P.; Sanders, H. M. H. F.; Fytas, G.; Meijer, E. W. *J. Am. Chem. Soc.* **2005**, *127*, 10334.
- Banerjee, D.; Broeren, M. A. C.; van Genderen, M. H. P.; Meijer, E. W.; Rinaldi, P. L. *Macromolecules* **2004**, *37*, 8313.
- Wallace, K. J.; Belcher, W. J.; Turner, D. R.; Syed, K. F.; Steed, J. W. *J. Am. Chem. Soc.* **2003**, *125*, 9699.
- Boas, U.; Karlsson, A. J.; de Waal, B. F. M.; Meijer, E. W. *J. Org. Chem.* **2001**, *66*, 2136.
- Pittelkow, M.; Christensen, J. B.; Meijer, E. W. *J. Polym. Sci., Part A Polym. Chem.* **2004**, *42*, 3792.
- Traficante, D. D. In *Encyclopedia of Nuclear Magnetic Resonance*; Grant, D. M., Harris, R. K., Eds.; Wiley: New York, 1996; Vol. 6, p 3988.

- (47) Imaoka, T.; Tanaka, R.; Yamamoto, K. *Chem.--Eur. J.* **2006**, *12*, 7328.
- (48) HyperChem(TM) Professional 8.0.8, Hypercube, Inc.: Gainesville, FL
- (49) Teobaldi, G.; Zerbetto, F. *J. Am. Chem. Soc.* **2003**, *125*, 7388.
- (50) Huissmann, S.; Likos, C. N.; Blaak, R. *J. Mater. Chem.* **2010**, *20*, 10486.
- (51) Liu, Y.; Bryantsev, V. S.; Diallo, M. S.; Goddard, W. A. *J. Am. Chem. Soc.* **2009**, *131*, 2798.